

RACE-IT: A Reconfigurable Analog CAM-Crossbar Engine for In-Memory Transformer Acceleration

Lei Zhao*, Luca Buonanno*, Ron M. Roth*, Sergey Serebryakov*, Archit Gajjar*
John Moon*, Jim Ignowski*, Giacomo Pedretti*

*Artificial Intelligence Research Lab (AIRL), Hewlett Packard Labs, USA
Email: {lei.zhao, giacomo.pedretti}@hpe.com

Abstract—Transformer models represent the cutting edge of Deep Neural Networks (DNNs) and excel in a wide range of machine learning tasks. However, processing these models demands significant computational resources and results in a substantial memory footprint. While In-memory Computing (IMC) offers promise for accelerating Matrix-Vector Multiplications (MVMs) with high computational parallelism and minimal data movement, employing it for implementing other crucial operators within DNNs remains a formidable task. This challenge is exacerbated by the extensive use of Softmax and data-dependent matrix multiplications within the attention mechanism. Furthermore, existing IMC designs encounter difficulties in fully harnessing the benefits of analog MVM acceleration due to the area and energy-intensive nature of Analog-to-Digital Converters (ADCs).

To tackle these challenges, we introduce a novel Compute Analog Content Addressable Memory (Compute-ACAM) structure capable of performing various non-MVM operations within Transformers. Together with the crossbar structure, our proposed RACE-IT accelerator enables efficient execution of all operations within Transformer models in the analog domain. Given the flexibility of our proposed Compute-ACAMs to perform arbitrary operations, RACE-IT exhibits adaptability to diverse non-traditional and future DNN architectures without necessitating hardware modifications. Leveraging the capability of Compute-ACAMs to process analog input and produce digital output, we also replace ADCs, thereby reducing the overall area and energy costs.

By evaluating various Transformer models against state-of-the-art GPUs and existing IMC accelerators, RACE-IT increases performance by $10.7\times$ and $5.9\times$, and reduces energy by $1193\times$, and $3.9\times$, respectively.

I. INTRODUCTION

Transformer models [49] have gained immense popularity in the field of natural language processing [20], [26], computer vision [8], [24], recommendation systems [33], [48], etc., thanks to their remarkable ability to capture complex patterns in sequential and image data. However, the performance of Transformers comes at a cost: their appetite for computational resources and memory. These models often feature millions, if not billions, of parameters, demanding substantial computation and data movement. The sheer scale of Transformer-based architectures, exemplified by models like GPT-3 [3] and BERT [7], necessitates specialized hardware and high-capacity memory systems, presenting a significant challenge to deploy them at scale. As a result, efficiently processing Transformer models remains a crucial concern in the quest to unlock their full potential for a wider range of applications.

In-memory Computing (IMC) stands out as a promising solution to alleviate the computational and memory challenges posed by Transformer models [15], [23], [53], [56]. IMC involves performing computations directly within the memory, bypassing the need for frequent data movement between memory and the processing units, which is a significant bottleneck in traditional computing architectures. Emerging memories such as Resistive Random Access Memories (ReRAM) and Phase Change Memories (PCMs) offer a compelling avenue for IMC due to their non-volatile nature and high integration potential. Crossbar arrays of such emerging memories can efficiently map neural network weights in their conductance and accelerate a layer evaluation by parallel Matrix-Vector Multiplications (MVMs) in the analog domain [13]. High-performance silicon demonstrations of multi-core IMC accelerators with ReRAM [50] and PCM [21] have been recently presented, finally grounding years of research, in experimental measurements. However, one notable drawback is that these designs may not be optimally suited for critical operations like Softmax and data-dependent matrix multiplications, which are fundamental to the Transformer model’s architecture and performance. Addressing these limitations and optimizing IMC designs for these specific operations is a critical area of ongoing research to enhance the applicability of IMC in Transformer-based processing.

To address this challenge, existing IMC designs fall into four main approaches. The first employs a direct ad-hoc solution, integrating specialized CMOS operators customized for specific workloads, as seen in ISAAC [43]. However, this approach lacks flexibility, making the adoption of new operators challenging. The second approach, exemplified by the PUMA architecture [1], utilizes programmable Vector Functional Units (VFUs) to support a wide variety of operations but incurs a performance cost, particularly in data-dependent matrix multiplications within Transformer models. The third approach explores ReRAM’s potential for computing the NOR operation [2], [9], [19], [45], offering a convenient solution for diverse operations but with drawbacks such as slow write speed and poor endurance. The fourth approach employs content addressable memories (CAMs) [37], which have gained attention in hyper-dimensional computing and genomics. In CAMs, a given input is searched and its location, i.e. address, is returned. The address can then be used to access a conventional RAM. CAM-based IMC has recently

gained attention, accelerating, for example, hyper-dimensional computing [14] and genomics [10]. CAMs were also used as look-up tables [37] where the match output indexes a memory array that stores pre-computed results, such as the activations of DNNs. However, every computation requires two steps, a CAM search and a subsequent memory read, both contributing to latency and energy overheads. In addition, it is challenging to scale up for high parallelism due to the substantial area overhead of the memory array. Recently, ReRAM-based Analog CAMs (ACAMs) have also been proposed [22]. Each ACAM cell encodes a range and checks whether an analog input falls within the range. ACAMs are naturally suitable to accelerate decision trees and their ensemble, by mapping tree branches directly within their ranges [31], [32]. ACAMs have also been used to implement various single-operand operations [46], [58], while still adhering to the look-up table approach, resulting in marginal improvements.

In this paper, we present a new ACAM cell structure, called Compute-ACAM, to support computing a wide range of arbitrary operations. It directly outputs each bit of the result, eliminating the need for a memory array and surpassing the look-up table approach. By reprogramming the ranges stored in the cells, the same Compute-ACAM array can be reconfigured for different operations without requiring any hardware modifications. This characteristic positions it as an ideal solution to construct a reconfigurable architecture capable of supporting all operators in Transformer models and even future operators that have yet to be conceived. We also leverage ACAM’s capability of accepting analog input and producing digital output, to replace the Analog-to-Digital Converters (ADCs), which account for more than 30% of the area and 50% of the power in ReRAM-based accelerators. Notably, all operations implemented using Compute-ACAM occupy less area than their CMOS-based counterparts.

Leveraging Compute-ACAM, we present RACE-IT, a *Reconfigurable Analog CAM-crossbar Engine for In-memory Transformer acceleration*, an accelerator architecture capable of efficiently handling operations across the entirety of Transformer models. We employ a pipelined execution fashion to optimize for throughput. Beyond Transformer models, RACE-IT possesses the versatility to support a broad spectrum of DNN architectures, including those integrating future operators yet to be introduced. To validate the effectiveness of our approach, we compare RACE-IT against state-of-the-art GPUs and ReRAM-based accelerators. The experimental results demonstrate significant performance enhancements of $10.7\times$ and $5.9\times$, along with substantial energy savings of $1193\times$ and $3.9\times$, respectively.

In summary, this paper offers the following contributions:

- A novel ACAM-based computing structure (Compute-ACAMs) that supports arbitrary operations. To the best of our knowledge, this is the first CAM-based design that does not need a memory array for arbitrary computation. Its reconfigurability, small area, and fast execution speed open up a new paradigm for reconfigurable computation in DNN accelerators.

- An encoding-based optimization that reduces the number of Compute-ACAM arrays needed to perform computation. This is an essential part of the design to make the proposed Compute-ACAM structure smaller enough for massive replication to achieve high parallelism.
- A full-fledged reconfigurable accelerator with crossbars and Compute-ACAMs that can efficiently execute full Transformer models and even future operators without adding new specialized components.
- We benchmark RACE-IT against state-of-the-art GPUs and ReRAM-based accelerators, achieving substantial performance improvement and energy saving.

II. BACKGROUND

A. Crossbar-based MVM Computing Engine

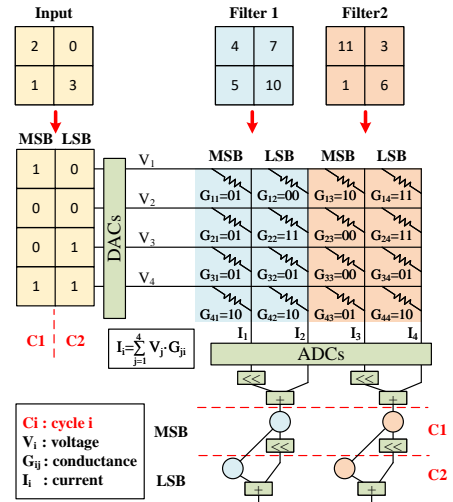


Fig. 1: ReRAM crossbar computing MVM with spatial bit slicing for weight and temporal bit slicing for input.

ReRAMs are emerging non-volatile memory with significant potential for accelerating MVMs when arranged in a crossbar structure. Figure 1 demonstrates computing a 4×4 input feature map with two 4×4 weight matrices mapped in ReRAM crossbar arrays. The input elements are transformed into a vector of voltages applied to the word lines. In contrast, weights are programmed as ReRAM conductance within the crossbar. Kirchhoff’s law ensures that the current flowing out on the bit lines represents the dot product between the input vector and the weight matrices. However, converting the analog current values back into the digital domain necessitates the use of ADCs that are area and power-expensive.

There is a disparity between the hardware resolution and algorithmic precision. DNN commonly needs 8 bits for inference [18], [25], [28], [40], [55]. While ReRAM cells have demonstrated programmability of up to 8 bits [44], it is often not possible to reach this precision on a large array due to stochastic variation of the device, such as drift and noise [30]. Furthermore, the resolution of word line voltages is limited due to hardware constraints related to Digital-to-Analog Converters (DACs). Therefore, a *bit slicing* [43] scheme is needed for both weights and input. In Figure 1, we assume a configuration of

2-bit input, 4-bit weights, 2-bit ReRAM cells, and 1-bit DACs. *Spatial bit slicing* is applied to weights by partitioning each weight into a 2-bit Most Significant Bit (MSB) part and a 2-bit Least Significant Bit (LSB) part. The MSBs and LSBs are stored in two cells located in adjacent columns. Consequently, the output from these columns is a partial sum that necessitates shifting and subsequent addition for consolidation. *Temporal bit slicing* is applied to input by sending each input bit to the crossbar over separate cycles. In practice, 1-transistor-1-resistor (1T1R) structures are employed to build the array, with the ReRAM biased at a fixed voltage and input bits applied on the access transistor gate. This also improves the reliability of matrix multiply to avoid errors due to the non-linear conductance of ReRAMs. Therefore, shift and add are also needed to aggregate the results from each cycle.

B. Analog Content Addressable Memory

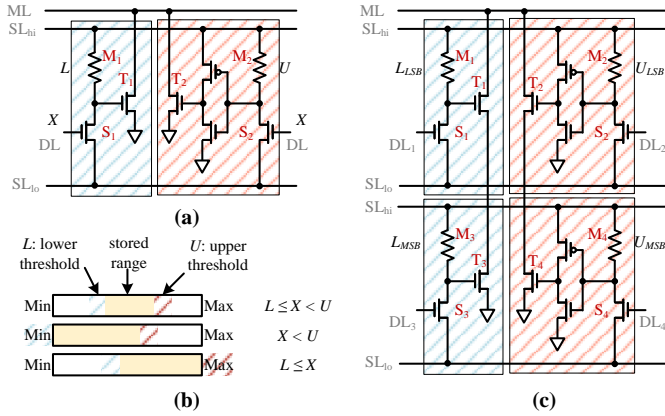


Fig. 2: (a) An ACAM cell structure. (b) An ACAM cell’s operational principle. (c) Increased-precision ACAM cell structure

A conventional digital CAM cell is limited to comparing a single binary input bit with a stored binary value. Ternary CAMs (TCAMs) have also been proposed, in which a wildcard ‘X’ can be used both as input or stored value, to match either 1s or 0s. The recently proposed ACAM cell structure [22] allows comparing an analog input value within a defined range stored in the cell. Figure 2(a) presents the schematic of an ACAM cell. Two memristors, M_1 and M_2 , are utilized to store the lower and upper thresholds, respectively. The blue-shaded area compares the input with the lower threshold of the range, while the red-shaded part compares the input with the upper threshold of the range. The combined operation of the series transistors (S_1 and S_2) and memristors act as voltage dividers, controlling the voltage supplied to the pull-down transistors (T_1 and T_2). In the blue-shaded section, when the input on the Data Line (DL) is greater than or equal to the data stored in M_1 , T_1 is off, thus keeping the Matching Line (ML) at a high voltage. The red-shaded portion operates similarly, with an inverter added before the pull-down transistor T_2 . Figure 2(b) illustrates the operational principle of an ACAM cell. It is possible to represent a “Don’t Care” value on either side of the range threshold by programming M_1 (M_2) to the lowest (highest) possible resistance, as depicted by the lower two rows

in Figure 2(b). Studies have demonstrated up to 4-bit analog search in ACAM [22], [31].

Figure 2(c) shows an extended cell that facilitates 8-bit comparisons [32], to accommodate the typical 8-bit precision requirement of many machine learning algorithms. This advanced structure comprises two original ACAM cells interconnected. Inputs, lower and upper thresholds are divided into a 4-bit Most Significant Bit (MSB) part and a 4-bit Least Significant Bit (LSB) part and are compared separately. By exploiting pull-down logic and re-use of pre-charged match lines, the overall match operation is reconstructed with two cycles.

C. Transformers and Multi-Head Attention

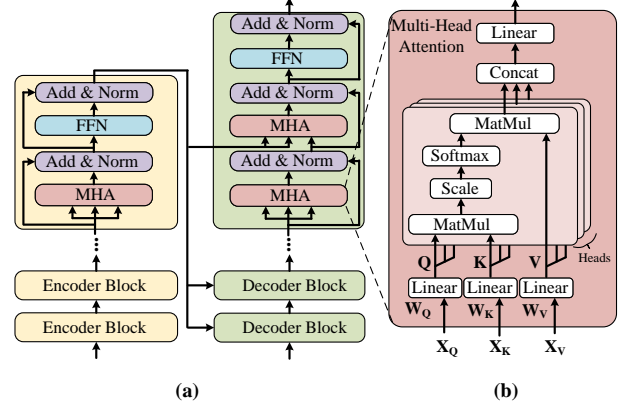


Fig. 3: (a) Transformer structure. (b) Multi-head attention.

1) *Transformer Model Structure*: Transformer models consist of both an encoder stack and a decoder stack [49], sharing a fundamental architecture showcased in Figure 3(a). Typically, the encoder processes the input sequence, and the decoder generates the output sequence. However, depending on the specific machine learning task, models might solely include either the encoder stack [5], [7], [20], [26], [41] or the decoder stack [6], [16], [34], [35]. Each encoder/decoder block comprises two key modules: the Multi-Head Attention (MHA) and the Feed-Forward Network (FFN). Subsequent to each module, a residual block aggregates the input and output from its previous MHA or FFN, transmitting the sum to a normalization layer. The contrast between an encoder block and a decoder block lies in an additional MHA, accompanied by its respective residual block and normalization layer within the decoder block. This additional MHA in the decoder block, apart from utilizing the output from its preceding MHA or FFN as input, also incorporates features from the last encoder block of the encoder stack.

2) *Multi-Head Attention*: The most fundamental component of Transformer models is the MHA, depicted in Figure 3(b). MHA operates on a sequence of tokens as its input, comprising three types of token sequences: the query token sequence X_Q , the key token sequence X_K , and the value token sequence X_V . Generally, these three token sequences are identical, except for the decoder block’s additional MHA, which employs the output of the encoder stack as the query and key token sequences. For each of these token sequences,

a distinct linear layer (denoted by \mathbf{W}_Q , \mathbf{W}_K , and \mathbf{W}_V in Figure 3(b)) is applied to generate respective matrices: a query matrix \mathbf{Q} , a key matrix \mathbf{K} , and a value matrix \mathbf{V} . This operation is defined as:

$$\mathbf{Q}, \mathbf{K}, \mathbf{V} = \mathbf{X}_Q \cdot \mathbf{W}_Q, \mathbf{X}_K \cdot \mathbf{W}_K, \mathbf{X}_V \cdot \mathbf{W}_V \quad (1)$$

These resulting matrices are then partitioned into multiple segments, often referred to as *heads*, which undergo identical sets of computations, specifically the attention mechanism, expressed as:

$$\text{Attention}(\mathbf{K}_i, \mathbf{Q}_i, \mathbf{V}_i) = \text{softmax} \left(\frac{\mathbf{Q}_i \cdot \mathbf{K}_i^T}{\sqrt{d_k}} \right) \cdot \mathbf{V}_i \quad (2)$$

where $i \in \text{num_heads}$, and d_k represents the dimension of a query and key vector. Ultimately, the output from each head is concatenated and goes through another linear layer to form the overall output of this MHA.

III. COMPUTE-ACAM CELL STRUCTURE

A. General Computing with ACAM

We provide two examples to show the insights of performing one-variable and two-variable operations within ACAM. We utilize the S-I-F notation to represent the bit allocation for the sign, integer, and fraction parts of the fixed-point format. For instance, 1-1-2 signifies a 4-bit fixed-point format, where the MSB is designated as the sign bit, followed by 1 bit for the integer part, and the remaining 2 LSBs for the fraction part.

Figure 4(a)-(c) depicts an illustrative example of computing the GeLU function, which is the state-of-the-art activation used in Transformer models. We use the fixed point format of 1-0-3 for both input and output. Figure 4(a) showcases the first two columns presenting all possible binary (x_B) and decimal (x_D) values of the input, followed by columns listing the decimal output of the GeLU function (y_D) and their values after quantization to the 1-0-3 format ($Q(y_D)$). The final column displays the binary bits of $Q(y_D)$. Rather than storing all computed results ($Q(y_D)$) in a memory array, we seek the ACAM to directly output the binary bits of the results, employing the MLs to output each bit of $Q(y_D)$. The core concept involves using one row of ACAM cells to determine if the input falls into any of the ranges that set the specific output bit to 1. For example, grouping the 1s in the last column in Figure 4(a) (highlighted in red) reveals that the MSB of the output equals 1 when the input falls within the range of [-1, -0.125), indicated by the blue border. Figure 4(b) displays all combinations of input ranges, resulting in each output bit being 1. Figure 4(c) demonstrates the mapping of the ranges in Figure 4(b) onto our *desired* ACAM array structure to execute this operation. This elucidates the first new requirement for our desired ACAM array structure, namely, *an OR operation is necessary for the cells along the same ML*. However, the original ACAM array could only execute an AND operation along the ML.

Figure 4(d)-(f) showcases a two-variable multiplication operation. For the sake of brevity, we adopt a 2-bit multiplication

in this example to ensure the table fits into the figure conveniently. Both input variables, denoted as x and y , utilize the 1-0-1 format, while the resulting output z utilizes the 1-1-2 format. In contrast to the one-variable example, a thorough examination of all range combinations of x and y is necessary. For instance, one feasible input range that triggers the MSB of the output to assume 1 entails x within [-1, -0.5) **and** y within [0.5, 1), shown by the blue border in Figure 4(d). Consequently, this underscores the second imperative for our envisioned ACAM structure—specifically, *the need for an AND operation encompassing two ranges from distinct inputs within the same cell*.

B. Cell Structure

To simplify the array and cell structure, and satisfy the first requirement, we use a conventional AND-type pull-down logic but with a custom OR-type ACAM cell. Following De-Morgan’s Law, by inverting the output of the ML the overall operation is equivalent to implementing an OR-type pull-down logic with an AND-type ACAM cell. The schematic of the modified cell is presented in Figure 5(a). The blue-shaded subpart calculates the upper threshold, while the red-shaded subpart computes the lower threshold.

To meet the second requirement and perform two-variable computations, a direct approach involves serially stacking two cells. However, considering that most operations in DNNs necessitate a minimum of 8-bit precision, we designed a cell capable of performing both two-variable computation and double the precision of the cell, with a similar technique as the one in Figure 2(b). The finalized Compute-ACAM cell structure is illustrated in Figure 5(c).

This cell structure supports three distinct computing modes: 8-bit one-variable computing (Figure 5(c)), 4-bit one-variable computing (Figure 5(d)), and 4-bit two-variable computing (Figure 5(e)). Having two additional subparts compared to the original 8-bit precision ACAM cell structure in Figure 2(c), it possesses the advantage of executing 8-bit computations within a single cycle by storing $U_{MSB} + 1$ and $L_{MSB} + 1$ in memristors, as depicted in Figure 5(c). For 4-bit computing on a single variable, only the middle two subparts are required. Consequently, the memristors in the top pair are set to the maximum resistance, while those in the bottom pair are set to the minimum resistance, rendering these two pairs as “Don’t Care” during computation, as illustrated in Figure 5(d). Figure 5(e) elucidates how this cell can be utilized to carry out computations on two 4-bit inputs. One subpart in each of the two pairs is designated as a “Don’t Care”, thus the remaining subparts are serially connected. Two of these subparts are allocated for the first input (X), and the remaining two are assigned to the second input (Y).

IV. COMPUTING WITH COMPUTE-ACAM

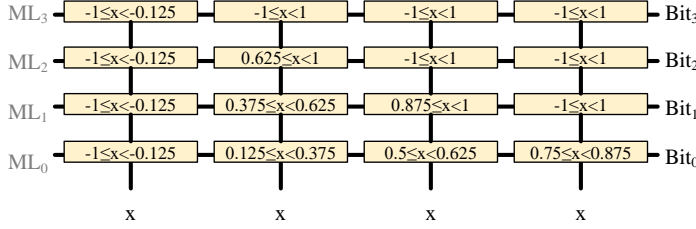
In this section, we elaborate on utilizing Compute-ACAM’s three computing modes to implement a diverse range of non-MVM operations within Transformer models.

x_B	x_D	y_D	$Q(y_D)$	$Q(y_D)_B$
1 0 0 0	-1	-0.1588	-0.125	1 1 1 1
1 0 0 1	-0.875	-0.1670	-0.125	1 1 1 1
1 0 1 0	-0.75	-0.17	-0.125	1 1 1 1
1 0 1 1	-0.625	-0.1662	-0.125	1 1 1 1
1 1 0 0	-0.5	-0.1542	-0.125	1 1 1 1
1 1 0 1	-0.375	-0.1326	-0.125	1 1 1 1
1 1 1 0	-0.25	-0.1003	-0.125	1 1 1 1
1 1 1 1	-0.125	-0.0562	0	0 0 0 0
0 0 0 0	0	0	0	0 0 0 0
0 0 0 1	0.125	0.0687	0.125	0 0 0 1
0 0 1 0	0.25	0.1496	0.125	0 0 0 1
0 0 1 1	0.375	0.2423	0.25	0 0 1 0
0 1 0 0	0.5	0.3457	0.375	0 0 1 1
0 1 0 1	0.625	0.4587	0.5	0 1 0 0
0 1 1 0	0.75	0.5799	0.625	0 1 0 1
0 1 1 1	0.875	0.7079	0.75	0 1 1 0

(a)

$Q(y_D)_B$	x_D
Bit ₃ =1	$-1 \leq x < -0.125$
Bit ₂ =1	$(-0.625 \leq x < -0.125) \vee (0.625 \leq x < 1)$
Bit ₁ =1	$(-0.625 \leq x < -0.125) \vee (0.375 \leq x < 0.625) \vee (0.875 \leq x < 1)$
Bit ₀ =1	$(-0.625 \leq x < -0.125) \vee (0.125 \leq x < 0.375) \vee (0.5 \leq x < 0.625) \vee (0.75 \leq x < 0.875)$

(b)



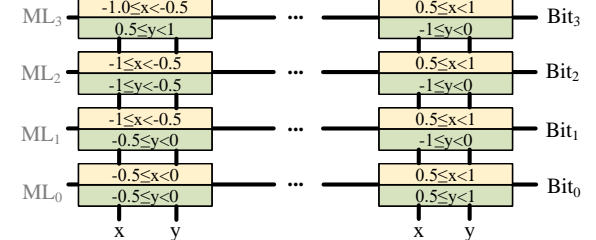
(c)

x_B	y_B	x_D	y_D	z_D	$Q(z_D)$	$Q(z_D)_B$
1 0	1 0	-1.0	-1.0	1.0	1.0	0 1 0 0
1 0	1 1	-1.0	-0.5	0.5	0.5	0 0 1 0
1 0	0 0	-1.0	0.0	0.0	0.0	0 0 0 0
1 0	0 1	-1.0	0.5	-0.5	-0.5	1 1 1 0
1 1	1 0	-0.5	-1.0	0.5	0.5	0 0 1 0
1 1	1 1	-0.5	-0.5	0.25	0.25	0 0 0 1
1 1	0 0	-0.5	0.0	0.0	0.0	0 0 0 0
1 1	0 1	-0.5	0.5	-0.25	-0.25	1 1 1 1
0 0	1 0	0.0	-1.0	0.0	0.0	0 0 0 0
0 0	1 1	0.0	-0.5	0.0	0.0	0 0 0 0
0 0	0 0	0.0	0.0	0.0	0.0	0 0 0 0
0 0	0 1	0.0	0.5	0.0	0.0	0 0 0 0
0 1	1 0	0.5	-1.0	-0.5	-0.5	1 1 1 0
0 1	1 1	0.5	-0.5	-0.25	-0.25	1 1 1 1
0 1	0 0	0.5	0.0	0.0	0.0	0 0 0 0
0 1	0 1	0.5	0.5	0.25	0.25	0 0 0 1

(d)

$Q(z_D)_B$	x_D & y_D
Bit ₃ =1	$[(-1 \leq x < -0.5) \wedge (-0.5 \leq y < 1)] \vee \dots \vee [(0.5 \leq x < 1) \wedge (-1 \leq y < 0)]$
Bit ₂ =1	$[(-1 \leq x < -0.5) \wedge (-1 \leq y < -0.5)] \vee \dots \vee [(0.5 \leq x < 1) \wedge (-1 \leq y < 0)]$
Bit ₁ =1	$[(-1 \leq x < -0.5) \wedge (-0.5 \leq y < 0)] \vee \dots \vee [(0.5 \leq x < 1) \wedge (-1 \leq y < 0)]$
Bit ₀ =1	$[(-0.5 \leq x < 0) \wedge (-0.5 \leq y < 0)] \vee \dots \vee [(0.5 \leq x < 1) \wedge (0.5 \leq y < 1)]$

(e)



(f)

Fig. 4: (a) Computing $y = GeLU(x)$ in ACAM as an example for one-operand computation. Assuming x and y are 4-bit fixed point data in 1-0-3 format. (b) Computing $z = x * y$ in ACAM as an example for two-operand computation. Assuming x and y are 2-bit fixed point data in 1-0-1 format, and z is a 4-bit fixed-point numbers in 1-1-2 format.

A. 4-bit One-Variable Computing (ADC)

Given that Compute-ACAM processes analog input and yields a digital output, it is well-suited to replace ADCs. Because an ADC transforms an analog representation into a digital one without altering the inherent value, we can construct a Compute-ACAM-based ADC in a similar approach as in Figure 4(a) by substituting the GeLU function with the Identity function ($y = x$). Utilizing the same crossbar configuration as in ISAAC [43] and PUMA [1], our Compute-ACAM-based ADC should maintain a precision equivalent to their ADCs, which is 8 bits. However, despite Compute-ACAM having an 8-bit one-variable computing mode, we could not use it for converting 8-bit analog data. This is because the 8-bit input needs to be partitioned into a 4-bit MSB part (X_{MSB}) and a 4-bit LSB part (X_{LSB}) before sending to the Compute-ACAM, as illustrated in Figure 5(c), whereas the output from the crossbar is a current representing a single 8-bit value.

To split the crossbar output to two 4-bit parts for Compute-ACAM, we propose a scheme similar to the one found in conventional folded ADCs. Figure 6 shows the conversion process. The conversion is divided into two successive steps. First, once the 8-bit analog data is ready from the crossbar for the conversion, the Compute-ACAM-based ADC is used

to convert the analog data as-is, resulting in the 4 MSB of converted digital result. In the second step, the DACs subtract an amount of signal equivalent to the 4 MSBs from the 8-bit analog value, and the subtraction result is rescaled in order to match Compute-ACAM's input dynamics; the Compute-ACAM-based ADC is then activated again, which results in the 4 LSB of the converted digital result.

B. 4-bit Two-Variable Computing (Multiplication)

Each MHA requires two data-dependent matrix multiplications, denoted by the \cdot operator in Equation 2. Different from MVM, both operands of data-dependent matrix multiplications are not fixed during inference. If we use the crossbar structure for data-dependent matrix multiplications, one of the operands needs to be written into the crossbar before each computation. However, this approach is susceptible to the long write latency and low endurance issues associated with ReRAM. We facilitate 4-bit multiplications by utilizing Compute-ACAM's 4-bit two-variable computing mode. An 8-bit multiplication can be decomposed into four 4-bit multiplications and three adds. Figure 4(b) has already demonstrated an example of 2-bit multiplication. Extending it to 4-bit multiplication is analogous, albeit necessitating a larger Compute-ACAM array to accommodate all the range combinations. Figure 7 illustrates the combinations of the two operands (x and y) that result in

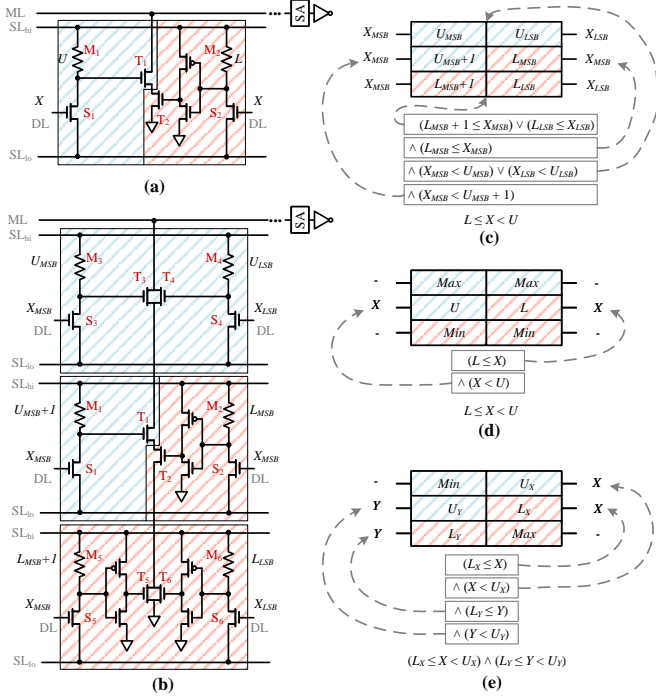


Fig. 5: (a) Modified conventional 4-bit ACAM cell to support OR operation among ranges. (b) Proposed 8-bit Compute-ACAM cell structure. (c) Mapping 8-bit comparison onto a Compute-ACAM cell. (d) Mapping 4-bit comparison onto a Compute-ACAM cell. (e) Mapping two-variable 4-bit comparison onto a Compute-ACAM cell.

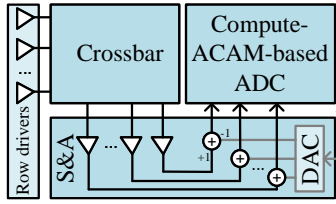


Fig. 6: Principle scheme of the analog S&A operation, enabling a 2-fold conversion of the 8-bit precision value from the crossbar.

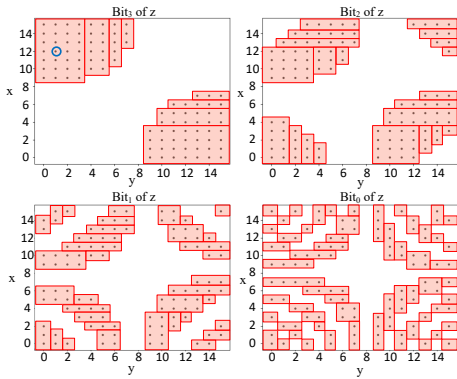


Fig. 7: Merging ranges for multiplication, assuming x and y is in 1-1-2 format, z is in 1-2-1 format.

each bit of the product (z) being equal to 1 (denoted by dots in the figure). For instance, the blue-circled dot in the top-left subfigure of Figure 7 demonstrates that the output's MSB (z_3) is 1 when $x = 12$ and $y = 1$. Since a cell stores a range of values, there is no need to individually program every dot in Figure 7 in a Compute-ACAM cell. Instead, we consolidate multiple dots into a single range if they can form a rectangle, and store this range in a single Compute-ACAM cell. For instance, the rectangle that contains the blue-circled dot could be programmed in one Compute-ACAM cell storing the range of $(9 \leq x < 16) \wedge (0 \leq y < 4)$. Therefore, the number of rectangles in each subfigure of Figure 7 determines the number of Compute-ACAM cells required to implement the 4-bit multiplication, i.e., computing z_3, z_2, z_1 and z_0 requires a row of 8, 21, 36 and 58 Compute-ACAM cells, respectively.

C. 8-bit One-Variable Computing (Softmax)

Softmax stands as a critical component within Transformer models, consuming approximately 20% to 40% of execution time on GPUs [4]. Even in specialized accelerators designed for Transformer models, Softmax remains a challenging design aspect due to its entailed exponentiation and division operations, both of which incur high hardware costs. The Softmax function is defined as follows:

$$\text{softmax}(x_i) = \frac{e^{x_i}}{\sum_{j=1}^L e^{x_j}} \quad (3)$$

Here, x_i represents an element in the input vector $\mathbf{X} = [x_1, \dots, x_L]$, and L denotes the input vector length.

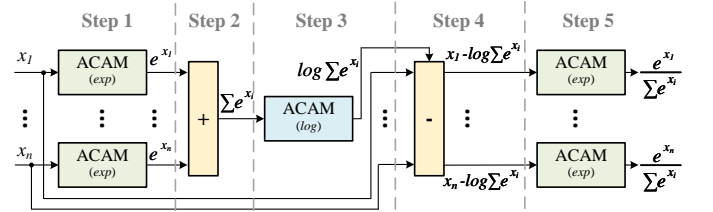


Fig. 8: Dataflow of computing Softmax using ACAM.

The expensive exponentiation and division operations can be easily mitigated with Compute-ACAM-based computing. Figure 8 portrays the dataflow of Compute-ACAM-based Softmax. We first leverage Compute-ACAM's 8-bit one-variable computing mode for exponentiation functions. Subsequently, these exponents are aggregated to yield the denominator in Equation 3. To circumvent the division operation and its associated hardware costs, we follow a similar approach as presented in [53], replacing division with logarithm, subtraction, and exponentiation based on the equivalence:

$$\frac{a}{b} = e^{(\log(a) - \log(b))} \quad (4)$$

The logarithm can be implemented like exponentiation within the 8-bit one-variable computing mode. Note that we do not need memory arrays to store pre-computed results for exponentiation and logarithm, resulting in a more compact and faster implementation compared to [53]. Given the strict

order of operations in Figure 8 due to data dependencies, most resources can be effectively reused. Notably, steps 1 and 5 can utilize the same set of Compute-ACAM arrays for computing the exponentiation, and since subtraction can be implemented with adders, steps 2 and 4 can share the same set of adders.

It is worth noting that the logarithm is undefined for input 0. Compute-ACAM does not need any specific hardware to handle this special case. Instead, we only need to hard set $\log(0) = m$ for the truth table of the logarithm, where m is the minimum value that can be represented by the data format of the output.

V. OPTIMIZING COMPUTE-ACAM ARRAY SIZE

To implement an arbitrary function using Compute-ACAM, the number of cells needed is determined by two key factors. The height (number of rows) is determined by the output width since each ML generates a binary bit for the output. The width (number of columns) is determined by the number of non-contiguous input ranges for each output binary bit, as contiguous ranges can be merged into a single range and stored in a single cell. Although the height is predetermined once the output bit width is established, there are opportunities to reduce the effective number of columns by merging more ranges. In this section, we propose two methods aimed at diminishing the number of Compute-ACAM cells needed to execute a function.

A. Encoding

Revisiting the last column of the table in Figure 4(a) reveals the potential for merging contiguous ranges, where the number of ranges for an output bit is determined by the count of runs of 1s. For an n -bit one-variable function, the total number of ranges is 2^n , reaching a worst-case scenario with interleaved 1s and 0s, resulting in 2^{n-1} runs of 1s. In Figure 7, the worst-case scenario for an output bit of a two-variable function (with operands of width m and n bits) is 2^{n+m-1} , with interleaved dots and blanks in the two-dimensional space. LSBs of the output exhibit a larger number of non-contiguous ranges due to increased toggle frequency as input values rise. Reducing the toggle rate of output bits enhances the potential for merging multiple ranges.

TABLE I: 4-bit Gray Code Encoding.

Decimal	Binary	Gray	Decimal	Binary	Gray
0	0000	0000	8	1000	1100
1	0001	0001	9	1001	1101
2	0010	0011	10	1010	1111
3	0011	0010	11	1011	1110
4	0100	0110	12	1100	1010
5	0101	0111	13	1101	1011
6	0110	0101	14	1110	1001
7	0111	0100	15	1111	1000

To minimize toggling in the LSBs, we adopt Gray Code for the output, as demonstrated in Table I for a 4-bit example. Originally designed to reduce error probabilities in analog-to-digital signal translation, Gray Code ensures only one bit changes at a time between consecutive numbers. This aligns

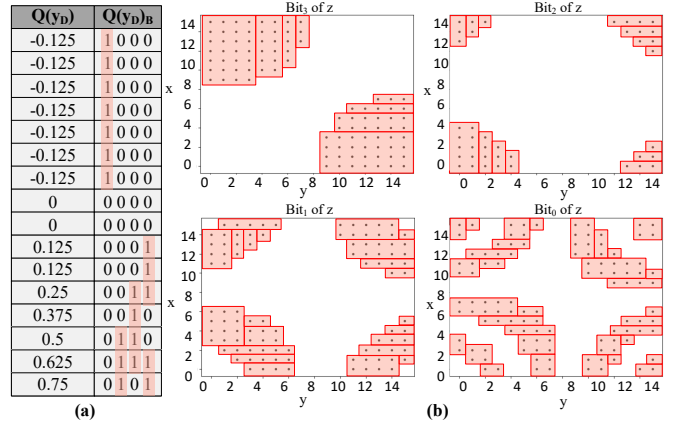


Fig. 9: (a) Merging ranges for 4-bit GeLU after applying Gray Code on output. (b) Merging ranges for 4-bit multiplication after applying Gray Code on output.

with our goal of reducing bit toggle frequency between consecutive numbers. Instead of producing the original binary output bits, Compute-ACAM outputs Gray Code encoded results. Figure 9 (a) and (b) display merged ranges after applying Gray Code encoding to 4-bit GeLU and multiplications in Section III-A. A comparison with the last column of the table in Figure 4(a) and Figure 7 reveals that encoding the output with Gray Code reduces the runs of 1s by roughly a factor of 2 for all output bits, except the MSB, which already exhibits the fewest ranges.

Because Compute-ACAM still takes original binary bits as input, we need to convert the Gray Code encoded output back to the original binary format before sending it for subsequent computations. The conversion process is very simple: each bit in the binary representation can be obtained by performing an XOR operation with all the higher-order bits in the Gray representation, except the MSB, which is the same between these two formats, i.e.,

$$b_i = \begin{cases} g_i & i = n - 1 \\ XOR(g_{n-1}, g_{n-2}, \dots, g_{i+1}) & i < n - 1 \end{cases}$$

where b_i and g_i are the i th bit in the binary and Gray Code format, respectively. n is the bit width of the output. Therefore, the conversion only needs some simple XOR gates.

B. Finer-Grained Compute-ACAM Array Size

Utilizing a single large array of Compute-ACAM cells to compute each output bit results in significant cell underutilization, especially for higher-order bits. Figure 10(a) shows cell utilization for Compute-ACAM-based 4-bit multiplication with encoding applied, revealing that 51% of cells (denoted in grey) remain unused, essentially functioning as a 'Don't Care' for input. These unused cells cannot be repurposed for other functions, as they cannot be excluded from participating in the computation of 4-bit multiplication.

To address this issue, we employ smaller-sized Compute-ACAM arrays and introduce reconfigurability for constructing larger arrays with non-uniform shapes. Multiple smaller-sized

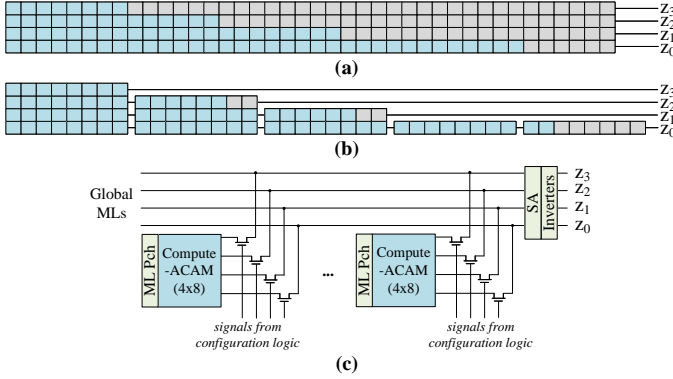


Fig. 10: (a) Implementing 4-bit multiplication with a single large array and (b) multiple small 4×8 arrays whose MLs can be individually connected. (c) A Compute-ACAM array group that supports configurable connection between rows from different arrays.

arrays are grouped together, allowing individual row configurations within each array to connect to the global ML with pull-down logic. Within the group, all arrays share the same set of sense amplifiers and inverters (Figure 10(c)). For example, with a 4×8 array size in Figure 10(b), 1 row is allocated for the MSB and 5 rows for the LSB, reducing unused cells to 12%. While small array size improves utilization, it increases hardware overhead due to complex control circuits. Compute-ACAM, supporting 4-bit and 8-bit computing modes, necessitates a minimum output bit width of 4 bits; reducing the row size below 4 does not enhance utilization. For a 4-bit input, the maximum non-contiguous range is 16, reducing to 8 after Gray Code encoding, leading us to choose a 4×8 array size in our design. The number of Compute-ACAM arrays in a group is determined by the worst-case number of cells needed to compute an output bit for an 8-bit one-variable function. After applying Gray Code encoding, an 8-bit one-variable function requires a maximum of 128 cells for one output bit, resulting in each Compute-ACAM group containing 16 arrays.

VI. ACCELERATOR ARCHITECTURE AND PIPELINE

Figure 11 illustrates the architecture of RACE-IT, with detailed parameters, area, and power specifications for each component listed in Table II. RACE-IT employs a two-level tile-core hierarchy, the same as in PUMA [1]. Each core has a multi-issue pipeline similar to that found in a superscalar CPU. The pipeline comprises three lanes, each capable of independently accepting new instructions. Data dependencies between these lanes are resolved during the compilation phase.

The Dot Product Engine (DPE) lane, similar to the MVM pipeline in PUMA and ISAAC, differs in its use of Compute-ACAM-based ADCs in RACE-IT. Because the amount of ADCs is determined by the number and size of crossbars, we reserve a fixed amount of Compute-ACAM arrays to be configured as ADCs, specifically, 256 arrays are configured into 256 4-bit ADCs, 32 for each crossbar. The configuration for crossbars and DACs follows ISAAC and PUMA, employing 128×128 crossbars with 1-bit DACs and 2-bit ReRAM cells.

TABLE II: RACE-IT parameters.

Component	Params	Spec	Power (mW)	Area (mm ²)
Core (12 cores per tile)				
DAC	resolution number	1bit 8 × 128	0.95532	0.00006
S&A	number	128	0.95	0.02064
Memristor Array	number size bits per cell	8 128 × 128 2	2.4	0.0002
Adder	number	1024	12.2281	0.01032
Register File	size	4KB	0.01573	0.00122
Control	-	-	0.0597	0.00135
XOR	number	6144	0.1536	0.00098
Compute-ACAM Array	number size bits per cell	1536 4 × 8 4	19.16928	0.10899
Core Total	-	-	35.93175	0.14378
Tile (121 tiles per chip)				
eDRAM Buffer	size num_banks bus_width	256KB 2 256bits	0.17308	0.08001
eDRAM-to-IMA bus	num_wire	384	1.67181	0.0369
Router	flit_size num_ports	32 8	10.03087	0.06191 (shared by 4 tiles)
Inst Mem	size	8KB	0.02721	0.0024
Control	-	-	0.11941	0.00059
Core	number	12	431.18	1.72547
Tile Total	-	-	435.68	1.86087
Chip				
Hyper Tr	links/freq link bw	4/1.6GHz 6.4GB/s	2.483K	9.3808
Tile	number	121	52.717K	225.16573
Chip Total	-	-	53.602K	203.17369

ISAAC’s weight encoding scheme is also adopted to reduce the precision for analog-to-digital conversion by 1 bit. The second lane consists of CMOS adders for handling additions in residual layers, Softmax, and data-dependent multiplications. We use CMOS adders because they offer excellent area and power efficiency after decades of optimization. The final lane is a reconfigurable General Computing Engine (GCE) composed of 1280 4×8 Compute-ACAM arrays.

We extend the instruction set of PUMA with a new `gce-compute` instruction:

```
gce-compute unit-id, src, dest, vec-width
```

The `unit-id` field specifies which computing unit configured from Compute-ACAM performs this computation. The source and destination register addresses are indicated by `src` and `dest` fields. `vec-width` field indicates the length of the vector operation.

To harness the computation parallelism provided by the multi-issue core, we carefully generate the instruction sequences for Transformer workloads to increase the utilization of all the lanes. The computation of MHA is divided into five stages, as illustrated in Figure 12. `mvm` stage computes one row of Q , denoted by $\mathbf{q} = \mathbf{X}_Q[q, :] \cdot \mathbf{W}_Q$. `matmul-1` stage performs data-dependent multiplications between \mathbf{q} and \mathbf{K} , i.e., $\mathbf{r} = \mathbf{q} \cdot \mathbf{K}^T$. `div-add` stage involves dividing and applying

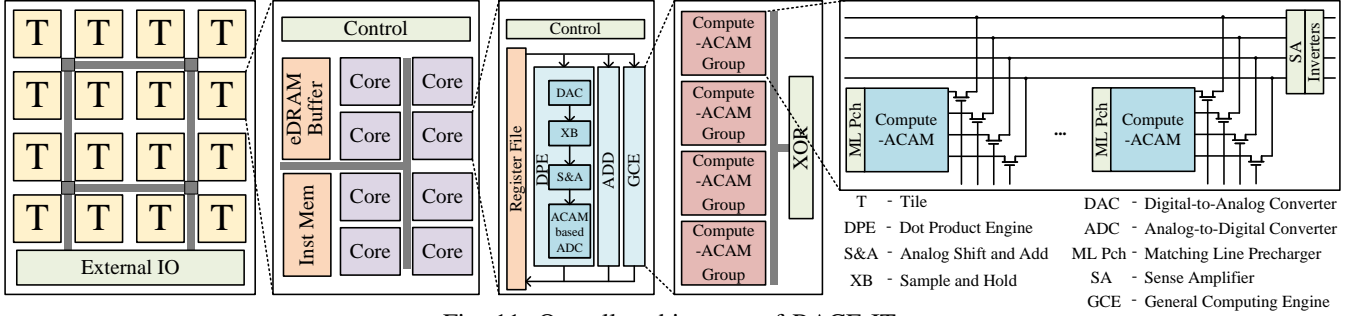


Fig. 11: Overall architecture of RACE-IT.

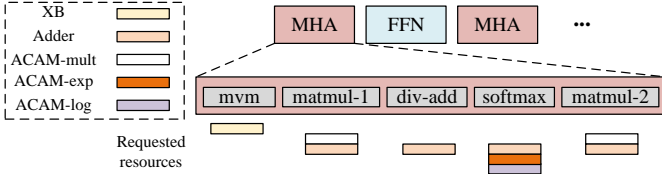


Fig. 12: Pipeline of RACE-IT for Transformer.

masks on \mathbf{r} . *softmax* stage computes the softmax on \mathbf{r} , resulting in $\mathbf{s} = \text{Softmax}(\mathbf{r})$. *matmul-2* stage computes another data-dependent multiplication between \mathbf{s} and \mathbf{V} , yielding the final output $\mathbf{out} = \mathbf{s} \cdot \mathbf{V}$.

A sequence of these five stages computing for the same \mathbf{out} is referred to as a *computing sequence*. As we process the rows of \mathbf{Q} sequentially, the computation of \mathbf{K} and \mathbf{V} for the next \mathbf{Q} can occur in parallel with the processing of the current \mathbf{Q} . The order of these five stages within a computing sequence must be preserved, but stages from different computing sequences can overlap since there are no data dependencies between them. In cases where two stages from different computing sequences request the same computing units, the later issued one will be stalled until the requested resource is available. The bottom part of Figure 12 shows the computing resources needed by each stage in MHA. Because a core has a large number of adders (1024), *matmul-1*, *div-add*, and *softmax* could use a different set of them.

The FFN only contains computation in conventional DNNs, such as linear layer, activation, residual, etc., which have been extensively explored to be implemented in ReRAM-based accelerators in prior works. The FFN and MHA can form another pipeline at an upper level. Compared to MHA, FFN involves considerably less computation, making this upper-level pipeline stage latency primarily determined by MHA.

VII. METHODOLOGY

We evaluated RACE-IT’s performance and energy efficiency by comparing it with two popular server-grade GPUs (NVIDIA P100 and H100 GPUs) and previous ReRAM-based accelerators that support Transformers. P100 GPU has 3,584 CUDA cores with 16 GB memory capacity, operating at a base frequency of 1.3 GHz, while the more recent H100 GPU has 6,144 CUDA cores with 32 GB memory capacity,

operating at a base frequency of 1.4 GHz. PUMA [1] is a programmable ReRAM-based accelerator equipped with general-purpose VFUs to facilitate the acceleration of diverse machine learning inference workloads, including Transformer models. ReTransformer [53] is a recent ReRAM-based accelerator designed explicitly for Transformers, utilizing crossbar functionality to compute data-dependent matrix multiplications. We scale up the number of VFUs in PUMA to match its chip area with that of RACE-IT and implement ReTransformer on top of PUMA without utilizing the VFUs during computation. Table III shows the significant differences between RACE-IT and the baseline ReRAM-based accelerators

TABLE III: Comparison to prior works.

Architecture	High-Cost ADC	Arbitrary ML	Program Crossbar	In-Memory Attention
PUMA [1]	Yes	Yes	No	No
ReTransformer [53]	Yes	No	Yes	Yes
RACE-IT	No	Yes	No	Yes

We expanded the capabilities of PUMAsim [1] to simulate RACE-IT and ReTransformer in a cycle-detailed manner. We use FinCACTI [42] to model the power and area for all SRAM buffers and eDRAM at 16nm. ACAM parameters are adopted from [22] and [31]. Other parameters are adopted from ISAAC and PUMA and scaled to 16nm according to [47]. All the parameters are listed in Table II. We use the CUDA event API in Pytorch to measure GPU performance and use NVIDIA-SMI [12], [29] to measure GPU power. The performance and power measurements are averaged across 30 runs, and we ignore the first run to mitigate the influence of library initialization and cache warmup.

We conducted tests on diverse Transformer models, including Bert-Base [7], Bert-Large [7], and GPT-2-Large [35]. Bert-Base is a moderate-size encoder-only model comprising 110 million parameters, while Bert-Large is a more extensive and computationally intensive model with 340 million parameters. GPT-2-Large, a decoder-only model, boasts a substantial parameter count of 1.5 billion. For models exceeding single-chip capacity, we distribute their weights across multiple RACE-IT chips. As RACE-IT processes the rows of \mathbf{Q} sequentially, a few hundred to one thousand bytes are generated at a time, which can be transferred in parallel with the computation of next row. The inter-chip connection bandwidth is 1.6GB/s, ensuring minimal throughput and energy overheads. Besides

Transformers, ResNet50 [11] was incorporated for benchmarking conventional CNN models. Pre-trained Transformer models on GLUE [51] and SQuAD [36] datasets were obtained from the Hugging Face Model Hub [52], and ResNet50 weights from TorchVision [39]. For accuracy metrics, we use Matthews correlation for CoLA, Pearson correlation for STS-B, F1 for SQuAD, and accuracy for all remaining tasks. Because the same Transformer model on different tasks only differs in the last linear layer (called classification head), we only report the performance and energy of the backbone of the Transformer models without the classification heads.

VIII. EXPERIMENTAL RESULTS

A. Evaluation of Compute-ACAM-base Computing Units

TABLE IV: Area and power Comparison between Compute-ACAM-based (w/ and w/o encoding) and CMOS-based operators.

Operator	Compute-ACAM			CMOS	
	Encode	Power (mW)	Area (μm^2)	Power (mW)	Area (μm^2)
4-bit ADC	No	0.012	70.9	0.113	116
	Yes	0.012	70.9		
4-bit Mult	No	0.053	301	0.00225	1104
	Yes	0.034	195		
8-bit GeLU	No	0.078	443	0.334	1054
	Yes	0.059	337		
8-bit Softmax	No	0.124	648	0.077	1131
	Yes	0.099	506		

Table IV compares the area and power consumption for multiple operators in Transformer models using Compute-ACAM-based computing in RACE-IT and conventional digital CMOS circuitry.

Parameters for the 4-bit ADC are adopted from [54], the GeLU unit is implemented using a non-uniform piecewise approximation [38], and parameters for the Softmax unit are adopted from [17]. All parameters are scaled down to 16nm. Across all operators, Compute-ACAM-based computing units are 39% to 82% smaller than their CMOS counterparts. Additionally, Compute-ACAM-based computing units exhibit lower power consumption, except for multipliers and Softmax units. The utilization of encoding yields a notable reduction in the area and power of Compute-ACAM-based operators, ranging from 22% to 35%. However, the 4-bit ADC does not exhibit a reduction in area and energy because the unencoded implementation already fits within one 4×8 Compute-ACAM array. As ADCs constitute the majority of power in ReRAM-based accelerators, RACE-IT maintains significantly higher power efficiency compared to other ReRAM-based accelerators, as detailed in Section VIII-B.

B. Performance and Energy

Figure 13(a) shows the speedup of all tested architectures normalized to P100 GPU. All three ReRAM-based designs surpass GPU baselines thanks to the enhanced MVM parallelism facilitated by the crossbar structure. RACE-IT significantly outperforms PUMA and ReTransformer for Transformer models. PUMA encounters computational bottlenecks

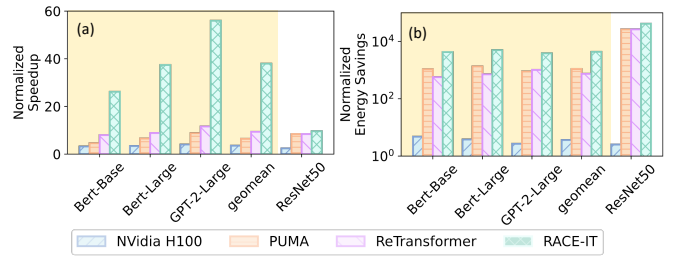


Fig. 13: (a) Inference speedup and (b) energy savings normalized to NVidia P100 GPU. The highlighted area shows the Transformer models performance.

as it performs data-dependent matrix multiplications within a limited number of VFUs. Despite we scaled up the number of VFUs in PUMA to match its chip area with that of RACE-IT for a fair comparison, each PUMA core still can only execute 64 multiplications at a time. Consequently, PUMA achieves just $6.4\times$ speedup over the P100 GPU on Transformer models. On the other hand, ReTransformer, which computes data-dependent matrix multiplications within the crossbar, offers higher computation parallelism but is constrained by the time-consuming crossbar write operation. Therefore, ReTransformer achieves $9.3\times$ speedup over the P100 GPU on Transformer models. RACE-IT optimizes the majority of its ACAMs as multipliers for data-dependent multiplications, achieving high computation parallelism (details on the balanced configuration can be found in Section VIII-D). In comparison to the P100 GPU, H100 GPU, PUMA, and ReTransformer, RACE-IT achieves speedups of $38\times$, $10.7\times$, $5.9\times$, and $4\times$, respectively. Note that larger models result in a larger speedup for RACE-IT, which can exploit at best the high parallelism. RACE-IT is still capable of accelerating conventional CNNs, with improved performance than PUMA and ReTransformer, because of much larger amount of activation units configured from ACAMs. As an example, we compared the inference of ResNet50 with the other architectures, showing $1.14\times$ speedup. Figure 13(b) shows the energy saving of all tested architectures normalized to P100 GPU. Once again, all three ReRAM-based architectures outperform GPU baselines in terms of energy saving. Notably, ReTransformer exhibits the highest energy consumption among those three due to frequent crossbar writes. Although ReTransformer employs a decomposed data-dependent multiplication strategy to mitigate the latency impact of excessive crossbar writes, it also reduces data reuse, thus increasing computational demands. RACE-IT achieves improved energy savings over PUMA and ReTransformer, primarily due to the elimination of conventional energy-intensive ADCs. Consequently, RACE-IT demonstrates the greatest energy savings for both Transformer models and CNNs. In comparison to PUMA and ReTransformer, RACE-IT achieves $3.9\times$ and $5.8\times$ more energy savings on Transformer models and $1.5\times$ more energy savings on ResNet50.

Table V shows the computation efficiency (TOPS) and energy efficiency (TOPS/W) of the three ReRAM-based architectures. RACE-IT achieves both the best computation

TABLE V: Comparison of Computation and Energy Efficiency.

Architecture	Bert-Base		Bert-Large		GPT-2-Large		ResNet50		Peak/Core	
	TOPS	TOPS/W	TOPS	TOPS/W	TOPS	TOPS/W	TOPS	TOPS/W	TOPS	TOPS/W
PUMA	19.27	27.48	33.59	34.87	42.16	18.59	3.33	128.88	6.31	130.21
ReTransformer	64.63	28	89.04	36.14	182.76	69.03	3.33	128.88	6.31	130.21
RACE-IT	110.11	109	191.90	129.1	268.2	80	3.8	194.14	7.07	196.94

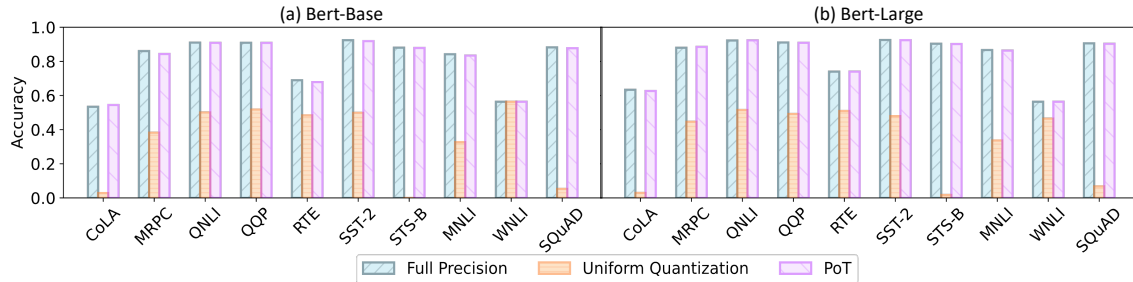


Fig. 14: Accuracy comparison for (a) BERT-Base and (b) BERT-Large for full precision, uniform quantization and Power of Two quantization

efficiency and energy efficiency for all benchmarks. RACE-IT has $1.12\times$ higher peak computation efficiency and $1.56\times$ higher peak power efficiency over PUMA and ReTransformer.

C. Accuracy

Given that ACAMs can only be configured to accept at most 8-bit operands, Transformer models need to be quantized. While the topic of quantization needs a separate paper to explore best practices for Transformers, this section focuses on delineating the unique quantization requirements of RACE-IT and presents an evaluation of one simple solution. Despite the widespread exploration of quantization techniques, the majority has primarily concentrated on CNNs, particularly in the quantization of layers with trainable weights. However, Transformer models involve numerous non-parameterized computations, such as data-dependent multiplication and Softmax, which also require quantization in RACE-IT. Figure 14 illustrates the accuracy of employing full-precision data-dependent multiplication and Softmax, along with the application of two different quantization schemes. Since RACE-IT computes Softmax in five steps (Figure 8), separate quantization is essential. However, straightforward application of uniform quantization yields poor accuracy, i.e., 47% accuracy loss. This is because uniform quantization assumes a uniform distribution on the underlying data, while the output of exponent functions (steps 1 and 5 in Figure 8) exhibit an exponential distribution. To address it, we utilized the Power of Two (PoT) quantization [27], [57], effectively resolving this issue. PoT quantizes values to the powers of two, particularly suited for value distributions with a sparse and power-law nature. We apply PoT on exponent functions and uniform quantization on all other operations, and the accuracy loss reduces to 0.2%. Importantly, since our ACAM can be configured for arbitrary functions, it is easy to support arbitrary non-uniform quantization schemes.

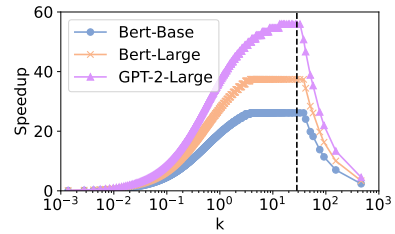


Fig. 15: Speedup over NVidia P100 GPU as a function of k , namely the ratio between the allocation of ACAMs as multipliers and exponential units. The dashed line shows our design choice.

D. GCE Configuration

Transformer models necessitate four types of computing units configured from GCE: multipliers for data-dependent multiplications, exponentiation units and logarithm units for Softmax, as well as activation units for computing the GeLU activation. From Figure 8, we know that only one logarithm operation is required for Softmax, while the number of exponentiation operations depends on the input size. Activation is only computed in FFN. As described in Section VI, FFN has much fewer computations compared to MHA and, therefore does not pose a critical impact on pipeline stage latency. Even with only one activation unit per core, FFN remains faster than MHA. Consequently, our exploration focuses on finding the optimal tradeoff between multipliers and exponentiation units, with logarithm units and activation units fixed at 1. We represent the ratio between multipliers and exponentiation units configured from GCE with k , ensuring it does not exceed the available Compute-ACAMs in the core. Figure 15 indicates that the optimal k falls between 3.7 to 38 for Bert-Base and Bert-Large and 13.4 to 38 for GPT-2-Large. For all benchmarks, we adopted $k = 28.3$, corresponding to 454 multipliers and 16 exponent units, denoted by the vertical line in the figure.

IX. CONCLUSION

In this paper, we present RACE-IT, a reconfigurable ReRAM-based accelerator for Transformer architectures. Our multi-lane ReRAM-based accelerator leverages a novel Compute-ACAM structure capable of computing arbitrary 4-bit and 8-bit one-variable, as well as 4-bit two-variable functions. It demonstrates superior performance, outpacing both GPU and existing ReRAM-based baselines by a significant margin. We demonstrate 10.7 \times and 5.9 \times speedup, 1193 \times and 3.9 \times increased energy efficiency compared with state-of-the-art GPU and IMC accelerators, respectively.

REFERENCES

- [1] A. Ankit, I. E. Hajj, S. R. Chalamalasetti, G. Ndu, M. Foltin, R. S. Williams, P. Faraboschi, W.-m. W. Hwu, J. P. Strachan, K. Roy *et al.*, "Puma: A programmable ultra-efficient memristor-based accelerator for machine learning inference," in *Proceedings of the Twenty-Fourth International Conference on Architectural Support for Programming Languages and Operating Systems*, 2019, pp. 715–731.
- [2] J. Borghetti, G. S. Snider, P. J. Kuekes, J. J. Yang, D. R. Stewart, and R. S. Williams, "'memristive' switches enable 'stateful' logic operations via material implication," *Nature*, vol. 464, no. 7290, pp. 873–876, 2010.
- [3] T. Brown, B. Mann, N. Ryder, M. Subbiah, J. D. Kaplan, P. Dhariwal, A. Neelakantan, P. Shyam, G. Sastry, A. Askell *et al.*, "Language models are few-shot learners," *Advances in neural information processing systems*, vol. 33, pp. 1877–1901, 2020.
- [4] J. Choi, H. Li, B. Kim, S. Hwang, and J. H. Ahn, "Accelerating transformer networks through recomposing softmax layers," in *2022 IEEE International Symposium on Workload Characterization (IISWC)*. IEEE, 2022, pp. 92–103.
- [5] K. Clark, M.-T. Luong, Q. V. Le, and C. D. Manning, "Electra: Pre-training text encoders as discriminators rather than generators," in *International Conference on Learning Representations*, 2020.
- [6] Z. Dai, Z. Yang, Y. Yang, J. G. Carbonell, Q. V. Le, and R. Salakhutdinov, "Transformer-xl: Attentive language models beyond a fixed-length context," in *Proceedings of the 57th Conference of the Association for Computational Linguistics, ACL 2019, Florence, Italy, July 28- August 2, 2019, Volume 1: Long Papers*. Association for Computational Linguistics, 2019, pp. 2978–2988.
- [7] J. Devlin, M.-W. Chang, K. Lee, and K. Toutanova, "BERT: Pre-training of deep bidirectional transformers for language understanding," in *Proceedings of the 2019 Conference of the North American Chapter of the Association for Computational Linguistics: Human Language Technologies, Volume 1 (Long and Short Papers)*. Association for Computational Linguistics, 2019, pp. 4171–4186.
- [8] A. Dosovitskiy, L. Beyer, A. Kolesnikov, D. Weissenborn, X. Zhai, T. Unterthiner, M. Dehghani, M. Minderer, G. Heigold, S. Gelly, J. Uszkoreit, and N. Houlsby, "An image is worth 16x16 words: Transformers for image recognition at scale," in *International Conference on Learning Representations*, 2021.
- [9] S. Gupta, M. Imani, and T. Rosing, "Felix: Fast and energy-efficient logic in memory," in *2018 IEEE/ACM International Conference on Computer-Aided Design (ICCAD)*. IEEE, 2018, pp. 1–7.
- [10] R. Hanhan, E. Garzón, Z. Jahshan, A. Teman, M. Lanuzza, and L. Yavits, "Edam: Edit distance tolerant approximate matching content addressable memory," in *Proceedings of the 49th Annual International Symposium on Computer Architecture*, ser. ISCA '22. New York, NY, USA: Association for Computing Machinery, 2022, p. 495–507. [Online]. Available: <https://doi.org/10.1145/3470496.3527424>
- [11] K. He, X. Zhang, S. Ren, and J. Sun, "Deep residual learning for image recognition," in *Proceedings of the IEEE conference on computer vision and pattern recognition*, 2016, pp. 770–778.
- [12] H. H. Holm, A. R. Brodtkorb, and M. L. Sætra, "Gpu computing with python: Performance, energy efficiency and usability," *Computation*, vol. 8, no. 1, p. 4, 2020.
- [13] M. Hu, J. P. Strachan, Z. Li, E. M. Grafals, N. Davila, C. Graves, S. Lam, N. Ge, J. J. Yang, and R. S. Williams, "Dot-product engine for neuromorphic computing: Programming 1t1m crossbar to accelerate matrix-vector multiplication," in *Proceedings of the 53rd Annual Design Automation Conference*, ser. DAC '16. New York, NY, USA: Association for Computing Machinery, 2016. [Online]. Available: <https://doi.org/10.1145/2897937.2898010>
- [14] M. Imani, A. Rahimi, D. Kong, T. Rosing, and J. M. Rabaey, "Exploring hyperdimensional associative memory," in *2017 IEEE International Symposium on High Performance Computer Architecture (HPCA)*, 2017, pp. 445–456.
- [15] M. Kang, H. Shin, J. Shin, and L.-S. Kim, "A framework for area-efficient multi-task bert execution on reram-based accelerators," in *2021 IEEE/ACM International Conference On Computer Aided Design (ICCAD)*. IEEE, 2021, pp. 1–9.
- [16] N. S. Keskar, B. McCann, L. R. Varshney, C. Xiong, and R. Socher, "CTRL: A conditional transformer language model for controllable generation," *CoRR*, vol. abs/1909.05858, 2019.
- [17] I. Kouretas and V. Paliouras, "Hardware implementation of a softmax-like function for deep learning," *Technologies*, vol. 8, no. 3, p. 46, 2020.
- [18] R. Krishnamoorthi, "Quantizing deep convolutional networks for efficient inference: A whitepaper," *arXiv preprint arXiv:1806.08342*, 2018.
- [19] S. Kvatinsky, G. Satat, N. Wald, E. G. Friedman, A. Kolodny, and U. C. Weiser, "Memristor-based material implication (imply) logic: Design principles and methodologies," *IEEE Transactions on Very Large Scale Integration (VLSI) Systems*, vol. 22, no. 10, pp. 2054–2066, 2013.
- [20] Z. Lan, M. Chen, S. Goodman, K. Gimpel, P. Sharma, and R. Soricut, "Albert: A lite bert for self-supervised learning of language representations," in *International Conference on Learning Representations*, 2020.
- [21] M. Le Gallo, R. Khaddam-Aljameh, M. Stanisavljevic, A. Vasilopoulos, B. Kersting, M. Dazzi, G. Karunaratne, M. Brändli, R. Singh, S. M. Müller, J. Büchel, X. Timoneda, V. Joshi, M. J. Rasch, U. Egger, A. Garofalo, A. Petropoulos, T. Antonakopoulos, K. Brew, S. Choi, I. Ok, T. Philip, V. Chan, C. Silvestre, I. Ahsan, N. Saulnier, V. Narayanan, P. A. Francese, E. Eleftheriou, and A. Sebastian, "A 64-core mixed-signal in-memory compute chip based on phase-change memory for deep neural network inference," *Nature Electronics*, vol. 6, no. 9, pp. 680–693, Sep. 2023. [Online]. Available: <https://doi.org/10.1038/s41928-023-01010-1>
- [22] C. Li, C. E. Graves, X. Sheng, D. Miller, M. Foltin, G. Pedretti, and J. P. Strachan, "Analog content-addressable memories with memristors," *Nature communications*, vol. 11, no. 1, p. 1638, 2020.
- [23] W. Li, M. Manley, J. Read, A. Kaul, M. S. Bakir, and S. Yu, "H3datten: Heterogeneous 3-d integrated hybrid analog and digital compute-in-memory accelerator for vision transformer self-attention," *IEEE Transactions on Very Large Scale Integration (VLSI) Systems*, 2023.
- [24] W. Li, H. Liu, R. Ding, M. Liu, P. Wang, and W. Yang, "Exploiting temporal contexts with strided transformer for 3d human pose estimation," *IEEE Transactions on Multimedia*, vol. 25, pp. 1282–1293, 2022.
- [25] T. Liang, J. Glossner, L. Wang, S. Shi, and X. Zhang, "Pruning and quantization for deep neural network acceleration: A survey," *Neuro-computing*, vol. 461, pp. 370–403, 2021.
- [26] Y. Liu, M. Ott, N. Goyal, J. Du, M. Joshi, D. Chen, O. Levy, M. Lewis, L. Zettlemoyer, and V. Stoyanov, "Roberta: A robustly optimized bert pretraining approach," *arXiv preprint arXiv:1907.11692*, 2019.
- [27] D. Miyashita, E. H. Lee, and B. Murmann, "Convolutional neural networks using logarithmic data representation," *arXiv preprint arXiv:1603.01025*, 2016.
- [28] M. Nagel, M. v. Baalen, T. Blankevoort, and M. Welling, "Data-free quantization through weight equalization and bias correction," in *Proceedings of the IEEE/CVF International Conference on Computer Vision*, 2019, pp. 1325–1334.
- [29] Nvidia, "Nvidia system management interface," <https://developer.nvidia.com/nvidia-system-management-interface>, 2019.
- [30] G. Pedretti, E. Ambrosi, and D. Ielmini, "Conductance variations and their impact on the precision of in-memory computing with resistive switching memory (rram)," in *2021 IEEE International Reliability Physics Symposium (IRPS)*, 2021, pp. 1–8.
- [31] G. Pedretti, C. E. Graves, S. Serebryakov, R. Mao, X. Sheng, M. Foltin, C. Li, and J. P. Strachan, "Tree-based machine learning performed in-memory with memristive analog cam," *Nature communications*, vol. 12, no. 1, p. 5806, 2021.
- [32] G. Pedretti, J. Moon, P. Bruel, S. Serebryakov, R. M. Roth, L. Buonanno, T. Ziegler, C. Xu, M. Foltin, J. Ignowski *et al.*, "X-time: An in-memory engine for accelerating machine learning on tabular data with cams," *arXiv preprint arXiv:2304.01285*, 2023.
- [33] C. Pei, Y. Zhang, Y. Zhang, F. Sun, X. Lin, H. Sun, J. Wu, P. Jiang, J. Ge, W. Ou *et al.*, "Personalized re-ranking for recommendation,"

- in *Proceedings of the 13th ACM conference on recommender systems*, 2019, pp. 3–11.
- [34] A. Radford, K. Narasimhan, T. Salimans, I. Sutskever *et al.*, “Improving language understanding by generative pre-training,” 2018.
- [35] A. Radford, J. Wu, R. Child, D. Luan, D. Amodei, I. Sutskever *et al.*, “Language models are unsupervised multitask learners,” *OpenAI blog*, vol. 1, no. 8, p. 9, 2019.
- [36] P. Rajpurkar, R. Jia, and P. Liang, “Know what you don’t know: Unanswerable questions for squad,” *arXiv preprint arXiv:1806.03822*, 2018.
- [37] M. S. Razlighi, M. Imani, F. Koushanfar, and T. Rosing, “Looknn: Neural network with no multiplication,” in *2017 Design, Automation & Test in Europe Conference & Exhibition (DATE)*. IEEE, 2017.
- [38] E. Reggiani, R. Andri, and L. Cavigelli, “Flex-sfu: Accelerating dnn activation functions by non-uniform piecewise approximation,” *arXiv preprint arXiv:2305.04546*, 2023.
- [39] F. A. Research, “Torchvision - pytorch vision library,” <https://github.com/pytorch/vision>, 2022.
- [40] B. Rokh, A. Azarpeyvand, and A. Khanteymooori, “A comprehensive survey on model quantization for deep neural networks in image classification,” *ACM Transactions on Intelligent Systems and Technology*, 2023.
- [41] V. Sanh, L. Debut, J. Chaumond, and T. Wolf, “Distilbert, a distilled version of bert: smaller, faster, cheaper and lighter,” *arXiv preprint arXiv:1910.01108*, 2019.
- [42] A. Shafaei, Y. Wang, X. Lin, and M. Pedram, “Fincacti: Architectural analysis and modeling of caches with deeply-scaled finfet devices,” in *2014 IEEE Computer Society Annual Symposium on VLSI*. IEEE, 2014, pp. 290–295.
- [43] A. Shafiee, A. Nag, N. Muralimanohar, R. Balasubramonian, J. P. Strachan, M. Hu, R. S. Williams, and V. Srikumar, “Isaac: A convolutional neural network accelerator with in-situ analog arithmetic in crossbars,” *ACM SIGARCH Computer Architecture News*, vol. 44, no. 3, pp. 14–26, 2016.
- [44] X. Sheng, C. E. Graves, S. Kumar, X. Li, B. Buchanan, L. Zheng, S. Lam, C. Li, and J. P. Strachan, “Low-conductance and multilevel cmos-integrated nanoscale oxide memristors,” *Advanced Electronic Materials*, vol. 5, no. 9, p. 1800876, 2019. [Online]. Available: <https://onlinelibrary.wiley.com/doi/abs/10.1002/aelm.201800876>
- [45] A. Siemon, S. Menzel, R. Waser, and E. Linn, “A complementary resistive switch-based crossbar array adder,” *IEEE journal on emerging and selected topics in circuits and systems*, vol. 5, no. 1, pp. 64–74, 2015.
- [46] T. Song, X. Chen, X. Zhang, and Y. Han, “Brahms: Beyond conventional rram-based neural network accelerators using hybrid analog memory system,” in *2021 58th ACM/IEEE Design Automation Conference (DAC)*. IEEE, 2021, pp. 1033–1038.
- [47] A. Stillmaker and B. Baas, “Scaling equations for the accurate prediction of cmos device performance from 180 nm to 7 nm,” *Integration*, vol. 58, pp. 74–81, 2017.
- [48] F. Sun, J. Liu, J. Wu, C. Pei, X. Lin, W. Ou, and P. Jiang, “Bert4rec: Sequential recommendation with bidirectional encoder representations from transformer,” in *Proceedings of the 28th ACM international conference on information and knowledge management*, 2019, pp. 1441–1450.
- [49] A. Vaswani, N. Shazeer, N. Parmar, J. Uszkoreit, L. Jones, A. N. Gomez, L. Kaiser, and I. Polosukhin, “Attention is all you need,” *Advances in neural information processing systems*, vol. 30, 2017.
- [50] W. Wan, R. Kubendran, C. Schaefer, S. B. Eryilmaz, W. Zhang, D. Wu, S. Deiss, P. Raina, H. Qian, B. Gao, S. Joshi, H. Wu, H.-S. P. Wong, and G. Cauwenberghs, “A compute-in-memory chip based on resistive random-access memory,” *Nature*, vol. 608, no. 7923, pp. 504–512, Aug. 2022. [Online]. Available: <https://doi.org/10.1038/s41586-022-04992-8>
- [51] A. Wang, A. Singh, J. Michael, F. Hill, O. Levy, and S. R. Bowman, “Glue: A multi-task benchmark and analysis platform for natural language understanding,” *arXiv preprint arXiv:1804.07461*, 2018.
- [52] T. Wolf, L. Debut, V. Sanh, J. Chaumond, C. Delangue, A. Moi, P. Cistac, T. Rault, R. Louf, M. Funtowicz *et al.*, “Huggingface’s transformers: State-of-the-art natural language processing,” *arXiv preprint arXiv:1910.03771*, 2019.
- [53] X. Yang, B. Yan, H. Li, and Y. Chen, “Retransformer: Reram-based processing-in-memory architecture for transformer acceleration,” in *Proceedings of the 39th International Conference on Computer-Aided Design*, 2020, pp. 1–9.
- [54] G. Yuan, P. Behnam, Z. Li, A. Shafiee, S. Lin, X. Ma, H. Liu, X. Qian, M. N. Bojnordi, Y. Wang *et al.*, “Forms: Fine-grained polarized reram-based in-situ computation for mixed-signal dnn accelerator,” in *2021 ACM/IEEE 48th Annual International Symposium on Computer Architecture (ISCA)*. IEEE, 2021, pp. 265–278.
- [55] X. Zhao, Y. Wang, X. Cai, C. Liu, and L. Zhang, “Linear symmetric quantization of neural networks for low-precision integer hardware,” in *International Conference on Learning Representations*, 2020.
- [56] Q. Zheng, S. Li, Y. Wang, Z. Li, Y. Chen, and H. H. Li, “Accelerating sparse attention with a reconfigurable non-volatile processing-in-memory architecture,” in *2023 60th ACM/IEEE Design Automation Conference (DAC)*. IEEE, 2023, pp. 1–6.
- [57] A. Zhou, A. Yao, Y. Guo, L. Xu, and Y. Chen, “Incremental network quantization: Towards lossless cnns with low-precision weights,” *arXiv preprint arXiv:1702.03044*, 2017.
- [58] H. Zhu, K. Zhu, J. Gu, H. Jin, R. T. Chen, J. A. Incorvia, and D. Z. Pan, “Fuse and mix: Macam-enabled analog activation for energy-efficient neural acceleration,” in *Proceedings of the 41st IEEE/ACM International Conference on Computer-Aided Design*, 2022, pp. 1–9.